REVISTA SOLDAGEM & INSPEÇÃO

ISSN 1980-6973 (Online) | ISSN 0104-9224 (Print)

ORIGINAL PAPER

Examination and Optimization of Friction Stir Welding Process Parameters of AA6092 Alloys

Umar Mohamed Jamaludeen[1]

[1] Annamalai Polytechnic College, Department of Mechanical Engineering, Chettinad, Tamil Nadu, India.

How to cite: Jamaludeen UM. Examination and optimization of friction stir welding process parameters of AA6092 alloys. Soldagem & Inspeção. 2024;29:e2907. https://doi.org/10.1590/0104-9224/SI29.07

Abstract: In this present examination, AA6092 alloys are friction-stir welded at various welding conditions to develop a welded joint with optimal ultimate tensile strength (UTS) and microhardness. This work deals with replacement of application of AA6061 alloys as bumper and bonnet by means of AA6092 alloys and this alloys tensile strength and microhardness is further increased by performing friction stir welding. This study investigates the performance of the friction stir welded butt joints of AA6092 alloys by varying the FSW process parameters such as tool rotational speed (TRS), welding speed (WS), axial load (AL), tool tilt angle (TTA), tool pin profile (TPP), shoulder diameter (SD), etc. In the current investigation, the empirical relationships are developed between most contributing FSW process parameters (TRS, WS, and AL) and their output responses (UTS and weld nugget microhardness (WNH)). The optimal UTS and WNH is predicted by the desirability approach of response surface methodology (RSM). The conforming values of input FSW process parameters are TRS of 1451.67 rpm, WS of 42.22 mm/min, and AL of 5.29 kN. For the existing examination, calculated UTS and WNH are 465.6 MPa and 151.8 HRB respectively, and the results of validation experiments are also invariable with these values.

Key-words: Friction stir welding; Ultimate tensile strength; Microhardness; Response surface methodology; Box-Behnken design; Optimization; Desirability approach.

1. Introduction

Bumper, Chassis front member, Bonnet and Fender are main parts of the car to prevent the accident in the automobiles. Recently aluminium and its alloys are the mostly employed materials to fabricate these automobile parts. Mostly AA6061 and AA6082 are used for bumper, fender and bonnet. These alloys are now replaced by AA6092 alloy due to its low density and high specific energy absorption performance and good specific strength that reduce the heavy damage during accidents. Since AA6092 alloy is alloyed with magnesium and silicon, they are easy to machine, weldable and precipitation hardened. The welding of this AA6092 alloy faces many difficulties like cracking, porosity and distortion while using traditional fusion welding processes.

To attain effectual defect-free joint on AA6092 alloys, Friction stir welding (FSW) is proved to be more competent and less costly solid state joining process for AA6092 Alloys. FSW has plentiful merits like energy efficient process, no fumes, arc flash or spatter, low distortion, low residual stresses and no need of shielding gas or filler material. These advantages of FSW have motivated numerous researchers to start and continue their research in the areas of modern shipbuilding, trains, automotive and aerospace industries. Researchers are developing innovative techniques and newer materials to optimize the performance of the FS welded joints. Advanced techniques are required for the optimization of mechanical properties (maximizing) such as UTS, WHN, etc. Response surface methodology (RSM) is one of the most precise methods for determining the optimum welding parameters with lesser time, no material wastage, and less human energies.

Recently some research studies are made to understand the effect of FSW on the mechanical characteristics of aluminium alloys. Guo et al. [1] in their paper investigated the FSW of dissimilar welding of AA6061 and AA7075 alloy with various FSW process parameters like WS, constant TRS, TTA, and AL. They concluded that both AA6061 and AA7075 alloys had shown a decrease in microhardness in the joints compared to base metals. They also reported that weld joints were failed at HAZ on the side of A6061 at the location of minimum microhardness. The highest UTS of 245 MPa was attained at the TRS, WS, AL, and TTA of 1200 rpm, 5 mm/s, 6.7 kN, 2.5º respectively. Sreenivas et al. [2] conducted the FSW on AA6082 T-6 using an H 13 steel tool with a threaded cylindrical pin profile by varying the AL, WS, and TRS as constants to explain the effect of the applied AL on the weld quality, weld strength, microstructural features and mechanical strength of welds generated. They informed that the maximum UTS (210 MPa) of the welds increased with AL up to 4 kN and hardness values at all the welds were slightly higher than the base alloy at nugget zones.

Received: 06 May, 2023. Accepted: 28 Feb., 2024.
E-mail: umarmjamaludeen@gmail.com (UMJ)

Farzadi et al. [3] employed the response surface methodology-based central composite design to optimize FSW operative parameters like TRS, WS, the shoulder diameter, and the pin diameter during FSW of AA7075. They concluded that the maximum joint strength (513 MPa) and maximum joint efficiency (94%) were obtained at the TRS of 513 rpm, WS of 95 mm/min, the shoulder diameter of 16.1 mm, and a pin diameter of 5 mm. Verma et al. [4] performed the central composite design (CCD) of response surface methodology (RSM) to optimize the FSW process parameters like TRS, WS, TTA for FSW of armor-marine grade AA7039 to measure the response parameters like UTS and tensile elongation. They adopted the desirability analysis for the optimization of process parameters. They reported that maximum joint efficiency of 2.5% higher than parent metal was achieved at TRS of 1325 rpm, WS of 35 mm/min, and TTA of 1.65º. They also concluded that the optimal condition for maximum UTS of 477 MPa and TE of 19.9% higher than base material was attained at TRS of 1337.5 rpm, WS of 37.5 mm/min, and TTA of 1.7º.

Arab and Zimri [5] carried out the FSW on AA6082-T6 plates using the FS welding tool made of tool steel with conical unthreaded pin profile and concave shoulder. They determined the effect of most important factors like TRS and WS on UTS and microhardness by the Taguchi L9 orthogonal array method. They concluded that the highest tensile strength of 202.05 MPa was obtained at optimum TRS and WS of 1400 rpm and 125 mm/min respectively. Khaki et al. [6] discussed the multi-objective optimization of the FSW parameters like TRS, WS, shoulder diameter concerning the pin diameter (D/d ratio), and TTA for AA6061-T6 to maximize the UTS and the surface hardness. They concluded that higher UTS of 190 MPa and higher surface hardness of 74.3 HV were attained at a TRS of 800 rpm, a D/d ratio of 3, a TTA of 7°, and a WS of 80 mm/min.

Mishra et al. [7] discussed on the optimization (single response) of FSW process parameters by employing a modified milling machine on AA6082-T6 and to find the parametric influence of TRS, WS, tool shoulder diameter, and tool pin's profile on UTS of the weld joint. They concluded that the TRS of 1200 rpm, WS of 30 mm/min, and tool of cylindrical threaded pin profile with shoulder diameter of 16 mm provide the optimal results of UTS of 245 MPa. Sameer and Birru [8] discussed the FSW between dual-phase 600 steel grade and AA6082-T6 using tungsten carbide tool by considering various TRS, WS, tool offsets, and constant TTA to study the macrostructure, microstructure, UTS, and microhardness of welded joints. They concluded that the highest UTS and joint efficiency obtained were 240 MPa and 85% respectively at the TRS of 710 rpm, WS of 40 mm/min, TTA of 0.5°, and tool pin offset of 1.3 mm. They concluded that the highest microhardness obtained was 246 HV in the stir zone.

Khanna et al. [9] focused on the optimization of FSW process parameters like TRS, TTA and WS for AA 8011-h14 using Taguchi analysis and studied the effect of these parameters on various properties like UTS, and microhardness. They concluded that the optimized parameters for higher UTS (84.44 MPa), and maximum microhardness (36.4 HV) were TRS of 1500 rpm, TTA of 1°, and WS of 50 mm/min. They also concluded that the higher temperature obtained on the advancing side was 389 °C at TRS of 1070 rpm, TTA of 2°, and WS of 50 mm/min. Maneiah et al. [10] discussed the FSW of AA6061-T6 alloy using H13 tool steel hexagonal pin taking the FSW process parameters such as TRS, TTA, WS and identifying the individual as well as simultaneous influences of FSW process parameters on the UTS of the FSW joints. They concluded that the highest UTS obtained was 191 MPa at TRS of 1400 rpm, TTA of 0º and WS of 100 mm/min.

Many research is being conducted by numerous researchers to optimize the responses (UTS, WNH, etc.) of the FSW joints of different aluminium alloys by identifying suitable process parameters, using nascent methods on novel and advanced materials. In this current work, examination have been performed on AA6092 alloy to improve the mechanical and metallurgical characteristics of the FS welded joints. Box-Behnken design and desirability approach of RSM have been adopted to develop empirical relationships between FSW process parameters (TRS, WS, and AL) and the two responses (UTS and WNH) and to determine the optimal welding conditions that will achieve FS weld butt joints with optimum UTS and WNH.

2. Experimental Work

2.1. Fabrication of tool for FSW

The tool steel H13 is the selected material for fabricating the non-consumable FSW tool. The chemical composition of this tool steel H13 is represented in Table 1. This tool is fabricated by having a cylindrical pin profile of size 5 mm with length of 4.8 mm and 15 mm shoulder diameter with the length of 12 mm as represented in Figure 1.

Table 1. Chemical Composition of tool steel H13.

Elements	Cr	Mo	Si	V	C
Content (%)	4.75-5.50	1.10-1.75	0.80-1.20	0.80-1.20	0.32-0.45
Elements	Ni	Cu	Mn	S	P
Content (%)	0.3	0.25	0.20-0.50	0.03	0.03

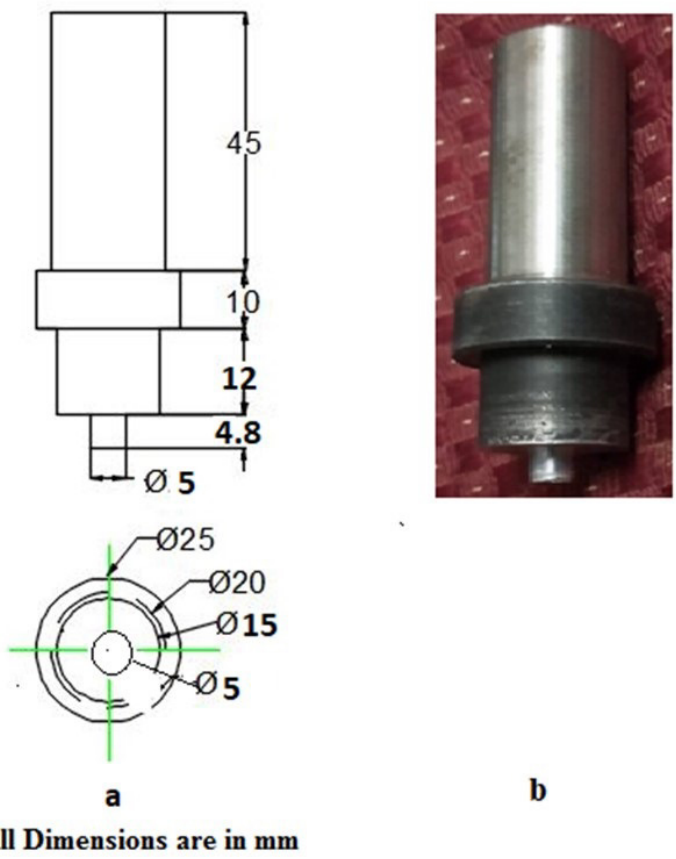

Figure 1. Details of FSW tool geometry. (a) 2-D Drawing of FSW tool; (b) Photograph of FSW tool.

2.2 Friction Stir Welding (FSW)

FSW is done on the two AA 6092 plates of dimensions 100 mm x 50 mm x 5 mm. The plates are fixed firmly in position in the FSW machine table by means of mechanical clamping. The rotational spindle of FSW machine is tightly fixed with a FSW tool (cylindrical pin profile). During FSW, the rotating tool is stirred vertically down for penetration and lengthwise for the joining of plates by employing a control panel. The hydraulic system of machine is employed to apply the axial load on the plates using FSW tool. In this present study, the major influencing process parameters considered are TRS, WS, and AL. The designated ranges of FSW process parameters and their levels are represented in Table 1. The minimum limit of a process parameter is represented as −1 and its maximum limit is represented as +1. An experimental design matrix is constructed using the Box-Behnken technique or model and it is represented in Table 2. FSW is conducted on AA6092 plates to produce the butt joints by varying the process parameters like TRS, WS, and AL as per the experimental design matrix shown in Table 3 and 4.

2.3 Welded joints characterization

After performing the friction stir welding, the welded joint is tested for its quality by conducting the tensile test, hardness tests, and metallographic tests. The test procedure for UTS measurement, weld nugget hardness measurement and microstructural examination for FS welded joint is explained in this section. The test specimens are prepared using a wire-cut Electrical Discharge Machining (EDM) as per ATSM standard. For tensile testing, the test specimens are cut perpendicular to the welded joint according to ASTM E8M-04 standards [11-13] as shown in Figure 2. The tests are conducted using a computer-controlled universal testing machine (Make: Associated Scientific Engg. Works, Model: F-100 and Capacity: Max 5 Ton). The UTS of the tensile specimen is calculated at 1 mm/min crosshead speed.

Weld nugget hardness testing has also been performed on Micro Vickers Hardness Tester (Make: Wilson Wolpert, Germany). Microhardness test specimens are fabricated according to the ASTM E10-08 standards [11-13] as shown in Figure 2. The weld nugget hardness is performed at three different locations of mid-thickness region of the weld nugget and the average value is employed for the analysis [14-17]. The transverse section of the welded plate is considered for the preparation of metallographic samples as shown in Figure 2. These samples are subjected to color etchant with a reagent (4 gm of $KMnO_4$ and 1 gm of NaOH dissolved in 100 ml distilled water). The metallurgical structure of the samples is visualized using an optical metallurgical microscope (De-Wintor Inverted Trinocular Metallurgical Microscope) and a Scanning Electron Microscope (FEI SEM-Apreo Model).

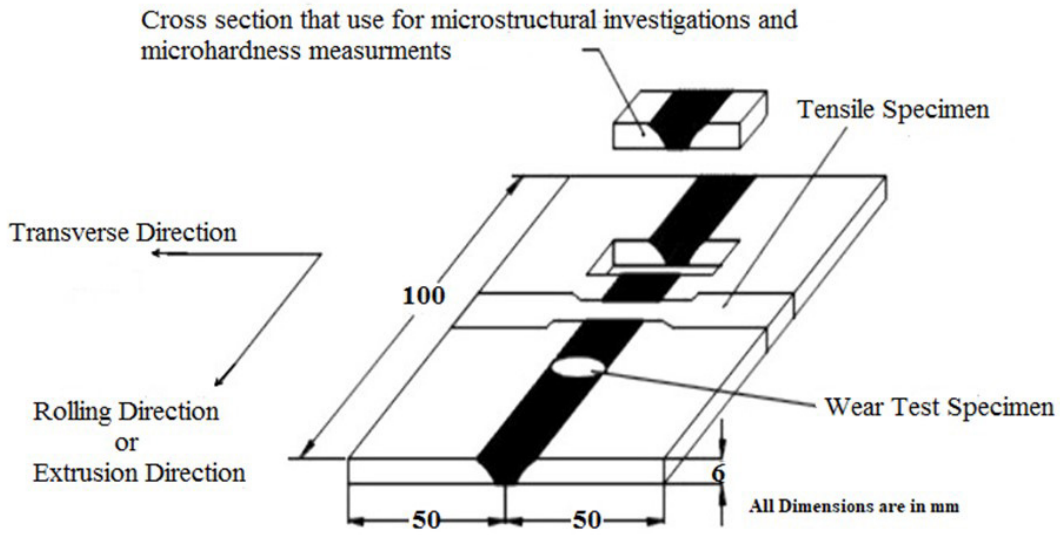

Figure 2. Schematic representations of specimen preparation for tensile test, microstructure, and hardness test on FS welded sample.

3. Analysis Methodology

3.1. Response surface methodology (RSM)

Engineers and Researchers always wish to obtain optimum values for output responses from the input process parameters or factors. The optimum values (maximum or minimum of a particular function) relies on the input factors. RSM is one of the highly efficient mathematical and statistical techniques employed for creating the empirical formula or model. Independent process variables are expressed quantitatively for experimental and in industrial situation are expressed as shown in Equation 1 [4,15].

$$Z = \psi (Y_1, Y_2, Y_3, ...Y_n) \pm \text{Error from the experiments} \quad (1)$$

Between the quantitative parameters, Y_1, Y_2, Y_3, ...Y_n and the response, Z, function 'ψ' is known as the response surface or function. The response surface corresponds to the certain set of independent process parameters. For a certain set of independent process parameters, a characteristic surface is retorted. The approximation using a polynomial is done agreeably for unidentified 'ψ' within the experimental area. In this investigation study, the RSM has been employed for the calculation of an empirical model using multiple regression equation for FSW of AA6092 for defining the quality characteristics of weldments. To implement the RSM, the independent parameter is considered as a surface for which an empirical model is fitted. UTS and WNH of the FSW of AA6092 are the functions of TRS, WS, and AL [14,15]. The surface can be expressed as follows:

$$UTS = f(TRS, WS, AL) \quad (2)$$

$$WNH = f(TRS, WS, AL) \quad (3)$$

The second-order polynomial (regression) equation is employed to denote the response surface is expressed by

$$X = a_0 + \Sigma a_i x_i + \Sigma a_{ii} x_i^{\,2} + \Sigma a_{ij} x_i x_j + \varepsilon \quad (4)$$

Second-order polynomial regression is employed to denote the 'X' response surface. Where a_0 is the average response; a_i, a_{ii} and a_{ij} are coefficients reliant on on the major and interaction influences of the parameters; and ε is the statistical error.

3.2. Box-Behnken design

In this current investigation, three FSW process parameters (TRS, WS, and AL) with three levels have been measured during the FSW of AA6092. The correlation of FSW process parameters (TRS, WS, and AL) with UTS and WNH of welded joints are usually established in the design before actual welding. In this examination, the Box-Behnken design approach has been adopted for evolving the correlation and to calculate the optimal design parameters for optimizing the UTS and WNH of FS welded joints. Three-factorial Box-Behnken experimental design has been nominated for defining the correlation between the response parameters (UTS and WNH) and the input parameters (TRS, WS, and AL). These most influencing process parameters of FSW on

the output responses have been identified with their levels using Box-Behnken model design and it is represented in Table 2. The levels of the FSW process parameters are indicated as 1 (high), 0 (medium) and –1 (low). According to Box-Behnken experimental design, seventeen experiments are to be conducted. Table 2 represents the actual design matrix.

3.3. Desirability approach

The desirability approach of RSM is used as most important technique for multiple response optimization problems or processes [14,15,18]. The importance of the desirability approach is that it offers equal importance to each and every single output response like UTS or WNH. In this current examination, multiple responses, such as UTS and WNH are transformed into a dimensionless parameter. The following Equation 5 provides the overall desirability function and is given by

$$\text{Desirability function } F = (d_1 * d_2 * ... * d_n)^{1/n} \quad (5)$$

where d_n indicates the desirability of the response and n is the number of responses.

Table 2. The level of process parameter.

FSW Process Parameters	Low	Medium	High
Tool Rotational Speed (rpm)	1000	1500	2000
Welding Speed (mm/min)	25	32.5	50
Axial Load (kN)	4	5	6

Table 3. Design matrix for FSW for AA6092.

Run	Tool Rotational Speed (rpm)	Welding Speed (mm/min)	Axial Load (kN)
1	1500	25	5
2	1500	37.5	5
3	2000	37.5	6
4	1000	50	5
5	2000	25	5
6	1500	25	4
7	1500	37.5	4
8	1000	37.5	6
9	1000	37.5	5
10	1500	37.5	6
11	1500	37.5	5
12	1500	50	6
13	1500	50	5
14	2000	25	4
15	1500	37.5	5
16	1000	37.5	4
17	2000	50	5

3.4. Optimization of process parameters

Design-Expert Software is employed for optimization of FSW process parameters of AA6092 alloys. Both numerical and graphical optimization methods of this software are used by setting the chosen goals for each input process parameter and response [14-16,18]. In the numerical optimization process, all the goals are combined into the overall desirability function. This optimization process set the minimum and maximum limits for each process parameters and determine the output response that will optimize the objective function. The graphical optimization method of this software is employed to find out the interaction effects of process parameters on output responses and it will be represented clearly in 2D contour plot and 3D contour plot. When dealing with a greater number of responses, numerical optimization is highly recommended and employed to calculate a practicable region whereas the graphical optimization aids to exhibit a achievable response area and lastly, the shaded region denotes the unfit optimization criteria. Figure 3 present the flow chart for both numerical and graphical optimization process of Design- Expert Software.

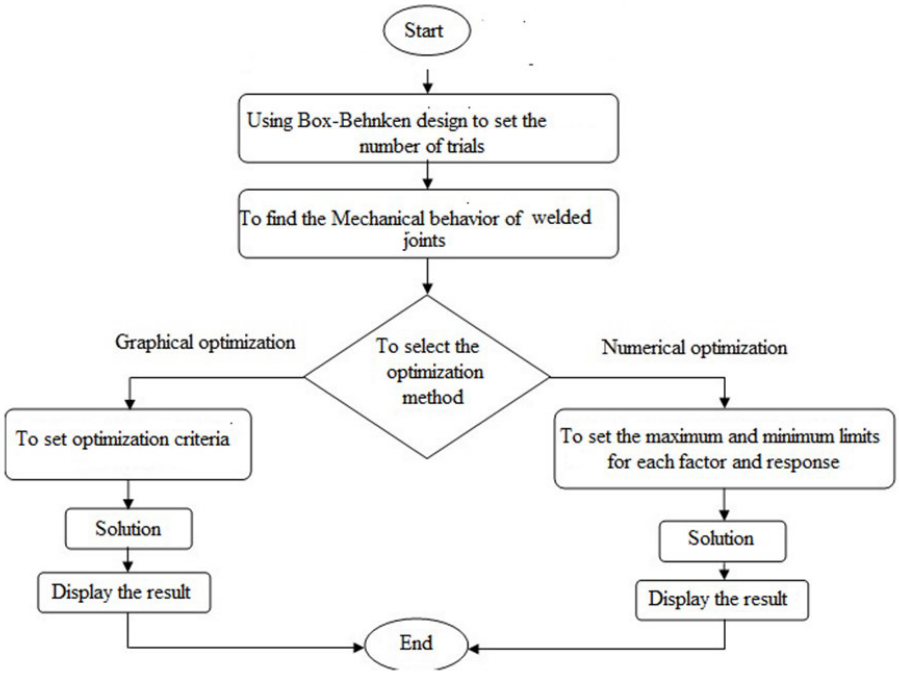

Figure 3. Flow chart for both numerical and graphical optimization process of Design-Expert Software.

4. Results and Discussion

4.1. Mechanical characterization

4.1.1. Developing empirical relationships

The tensile test and hardness test are done on the butt-welded joints as per ASTM E8M-04 standards [11-13] and ASTM E10-08 standards [11-13] respectively. UTS and WNH were calculated from each specimen and they are shown in Table 4 and these results are adopted to attain the empirical mathematical relations.

Table 4. Experimental Design matrix and Results of UTS and WNH.

Run	Tool Rotational Speed (rpm)	Welding Speed (mm/min)	Axial Load (kN)	Tensile strength (MPa)	Weld Nugget Micro-hardness (HRB)
1	1500	25	5	466	153
2	1500	37.5	5	465	152
3	2000	37.5	6	450	127
4	1000	50	5	452	142
5	2000	25	5	436	138
6	1500	25	4	458	143
7	1500	37.5	4	443	151
8	1000	37.5	6	452	141
9	1000	37.5	5	454	142
10	1500	37.5	6	466	153
11	1500	37.5	5	464	144
12	1500	50	6	466	152
13	1500	50	5	468	151
14	2000	25	4	456	123
15	1500	37.5	5	465	150
16	1000	37.5	4	454	146
17	2000	50	5	465	132

The final regression relations to compute the UTS and WNH of FS welded joint for AA6092 alloy are summarized as in Equations 6 and 7 respectively.

$$UTS = 358.7 + 0.07685 \times TRS - 1.176 \times WS + 25.125\ AL + 0.00124 \times TRS \times WS - 0.002 \times TRS \times AL + 0.3 \times WS \times AL - 3.8e\text{-}05 \times TRS^2 - 0.02752 \times WS^2 - 3.05 \times AL^2 \quad (6)$$

$$WNH = -39.775 + 0.13305 \times TRS + 0.472 \times WS + 36.125 \times AL - 0.00024 \times TRS \times WS + 0.0045 \times TRS \times AL - -2.32E\text{-}16 \times WS \times AL - 5.3E\text{-}05 \times TRS^2 - -0.00016 \times WS^2 - 4.275 \times AL^2 \quad (7)$$

ANOVA technique is employed for confirming the acceptance of final developed regression relationships. The developed model is accepted if the determined value of the F- ratio of the developed model is less than the standard F ratio value from the F table under the desired level of confidence (say 95%). Table 5 shows ANOVA results for Ultimate Tensile Strength (UTS). Table 6 shows ANOVA results for Weld Nugget Hardness (WNH).

Table 5. ANOVA results for Ultimate Tensile Strength (UTS).

Source	Sum of Squares	df	Mean Square	F-value	p-value	
Model	930.93	9	103.44	1.71	0.2454	not significant
A-Tool Rotational Speed	3.12	1	3.12	0.0517	0.8266	
B-Welding Speed	18.00	1	18.00	0.2979	0.6021	
C-Axial Load	66.13	1	66.13	1.09	0.3303	
AB	240.25	1	240.25	3.98	0.0864	
AC	4.00	1	4.00	0.0662	0.8043	
BC	56.25	1	56.25	0.9310	0.3668	
A^2	384.01	1	384.01	6.36	0.0398	
B^2	77.85	1	77.85	1.29	0.2937	
C^2	39.17	1	39.17	0.6483	0.4472	
Residual	422.95	7	60.42			
Lack of Fit	413.75	3	137.92	59.96	0.0009	significant
Pure Error	9.20	4	2.30			
Cor Total	1353.88	16				

Table 6. ANOVA results for Weld Nugget Hardness (WNH).

Source	Sum of Squares	df	Mean Square	F-value	p-value	
Model	1217.69	9	135.30	7.04	0.0087	significant
A-Tool Rotational Speed	325.12	1	325.12	16.91	0.0045	
B-Welding Speed	12.50	1	12.50	0.6503	0.4465	
C-Axial Load	0.1250	1	0.1250	0.0065	0.9380	
AB	9.00	1	9.00	0.4682	0.5158	
AC	20.25	1	20.25	1.05	0.3389	
BC	0.0000	1	0.0000	0.0000	10.000	
A^2	742.00	1	742.00	38.60	0.0004	
B^2	0.0026	1	0.0026	0.0001	0.9910	
C^2	76.95	1	76.95	4.00	0.0855	
Residual	134.55	7	19.22			
Lack of Fit	127.75	3	42.58	25.05	0.0047	significant
Pure Error	6.80	4	1.70			
Cor Total	1352.24	16				

4.1.2. The influence of the FSW process parameters on the responses (UTS and WNH)

In this segment, the interaction effects of two input process parameters on the output responses are measured with the third process parameter kept at an average level.

4.1.2.1. Ultimate tensile strength (UTS)

The perturbation plot (Figure 4) represents the influence of FSW process parameters on UTS for an optimized design. From this plot, it shows that response varies when each parameter transfers away from the common or reference points keeping all other process parameters constant at that reference point. It is also shows from this plot that the TRS is the highly dominating process parameter on UTS accompanied by WS and AL.

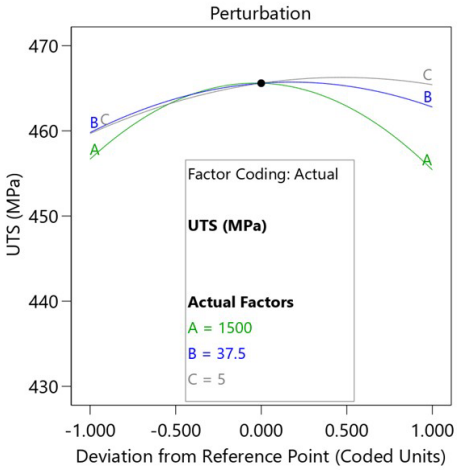

Figure 4. Perturbation plot (influence of FSW process parameters on the UTS).

The interaction effects of TRS, WS, and AL on the UTS are represented in Figures 5, 6, and 7. Figure 5a and b represent the influence of the TRS and WS on UTS by keeping AL 5 kN. The concentric circle in the 2D contour plot (Figure 5a) represent the tensile strength (MPa) and its optimum value is attained at the centre of this plot. The optimum UTS of 465 MPa (Figure 4A and B) is attained at a TRS of 1500 rpm and a WS of 37.5 mm/min.

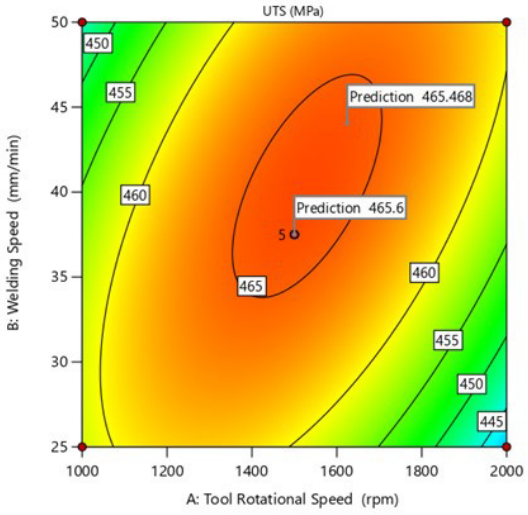

(a) 2D Contour plot

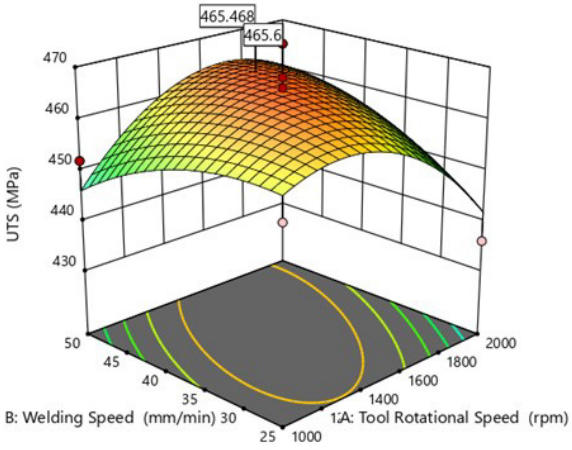

(b) 3D Contour plot

Figure 5. Contour plots (influence of TRS and WS on UTS of FSW Joint.

Figure 6 presents the interaction effect of AL along with TRS at constant WS of 37.5 mm/min. The optimum UTS is attained around 465 MPa (2D and 3D plots) at a TRS of 1500 rpm and an AL of 5 kN.

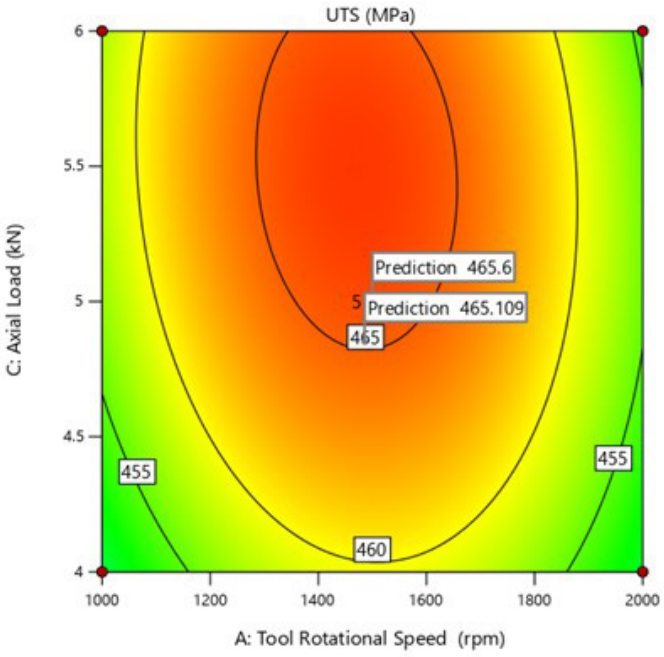

(a) 2D Contour plot

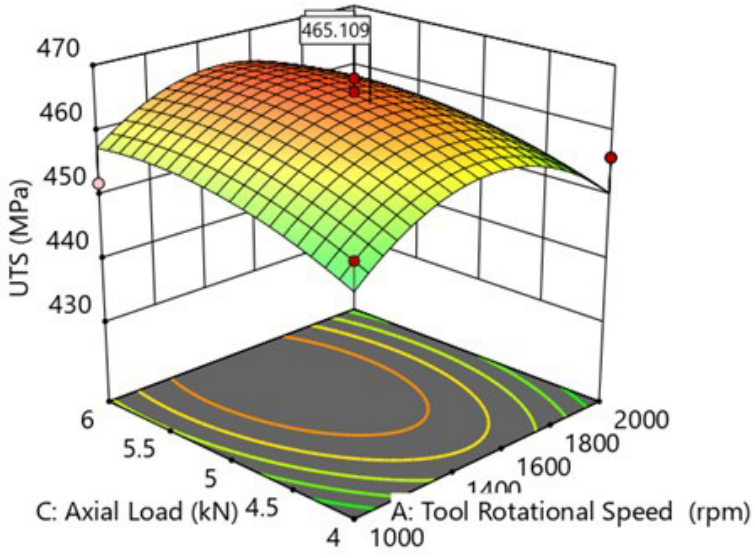

(b) 3D Contour plot

Figure 6. Contour plots (influence of TRS and AL on UTS of FSW Joint.

Figure 7 represents the interaction effect of AL along with WS at constant TRS of 1500 rpm. The approximate value of the optimum UTS of 465.6 MPa (2D and 3D plots) is obtained at a WS of 37.5 mm/min and an AL of 5 kN.

The base AA6092 alloy accounts microhardness of 147 HRB which is lower than that of stir zone. The weld nugget hardness consistently surpasses that of the base metal, regardless of the tool's rotational speed. This disparity in hardness can be attributed to two primary factors contributing to the enhancement of weld nugget hardness. Firstly, the grain size within the stir zone is significantly finer compared to the base metal. This refinement of grain size is

instrumental in bolstering the material's overall strength, aligning with the principles outlined in the Hall-Petch equation, which establishes a direct correlation between decreasing grain size and increasing hardness. Secondly, the presence of minuscule intermetallic particles and uniformly dispersed SiC_p within the weld nugget further augments its hardness, owing to the mechanisms of Orowan hardening. The contrast in hardness between the heat-affected zone (HAZ) and the stir zone can be ascribed to the grain refinement process taking place specifically within the stir zone. Figure 8 (perturbation plot) represents the influence of FSW process parameters on WNH for an optimized design. For every working level of TRS, WNH remains to be greater than that of base metal.

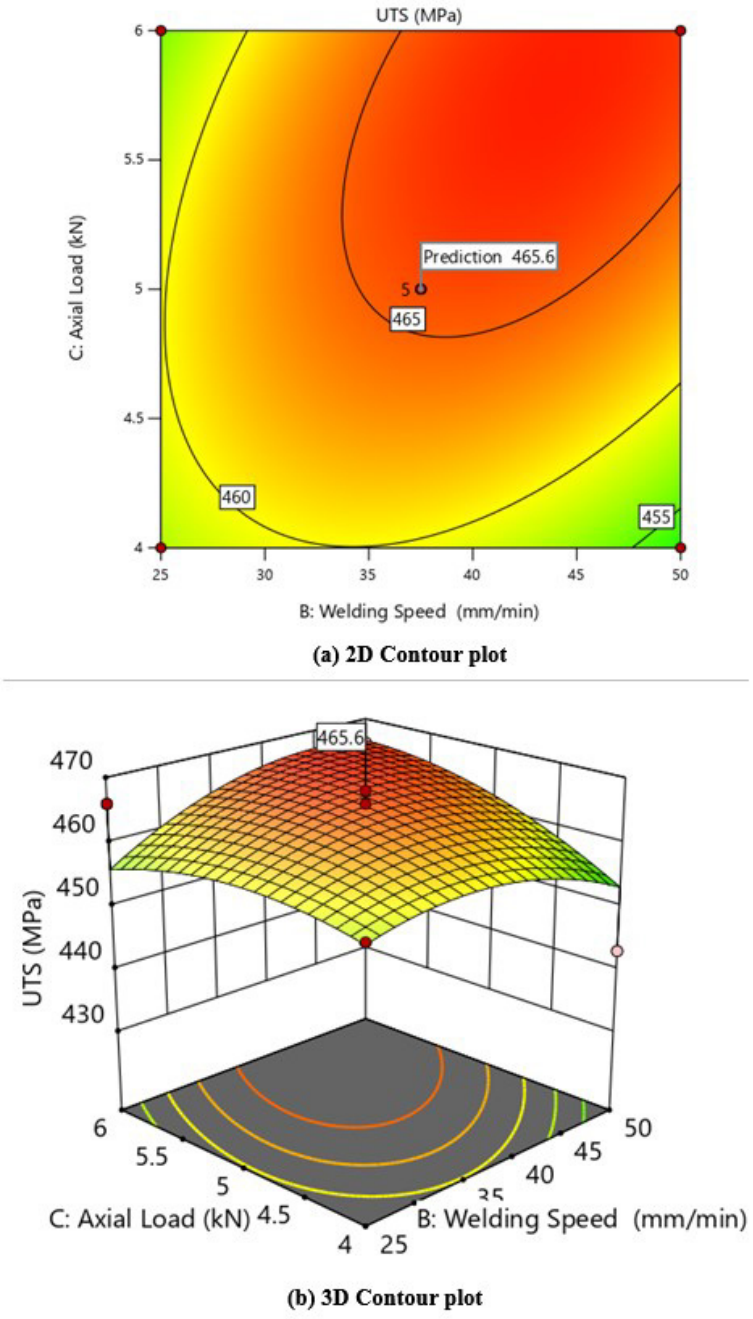

(a) 2D Contour plot

(b) 3D Contour plot

Figure 7. Contour plots (influence of WS and AL on UTS of FSW Joint.

4.1.2.2. Weld nugget micro-hardness (WNH)

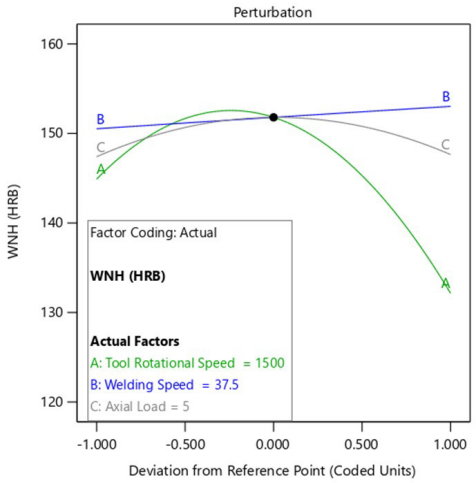

Figure 8. Perturbation plot (influence of FSW parameters on WNH).

The interaction effects of TRS, WS, and AL on the WNH are represented in Figures 9, 10, and 11. Figure 9a and b represent the influence of the TRS and WS on WNH by keeping AL 5 kN. The concentric circle in the 2D contour plot (Figure 9a) represent the hardness (HRB) and its optimum value is attained at the centre of this plot. The optimum WNH of 153 HRB (Figure 9a and b) is attained at a TRS of 1500 rpm and a WS of 37.5 mm/min.

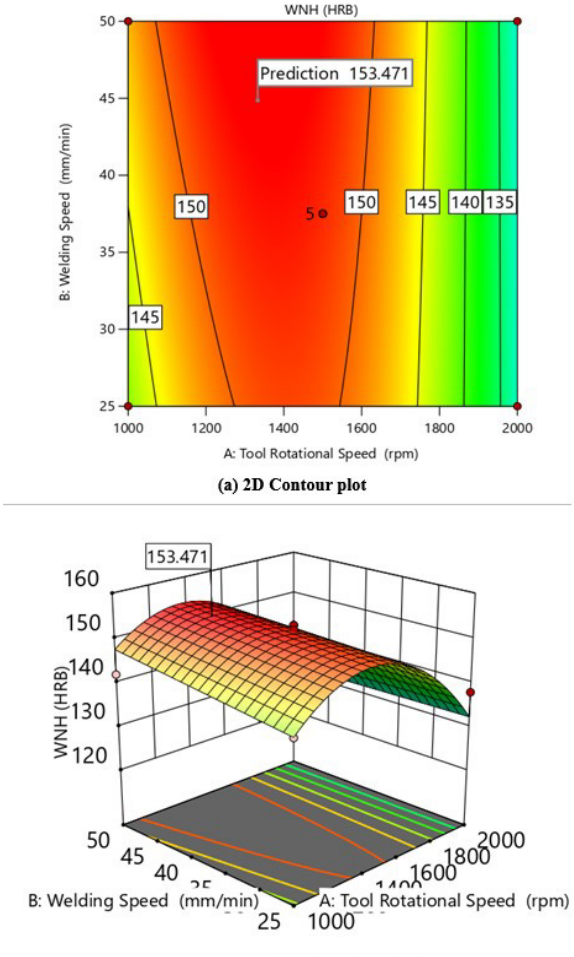

Figure 9. Contour plots (influence of TRS and WS on WNH.

Figure 10 presents the interaction effect of AL along with TRS at constant WS of 37.5 mm/min. The optimum WNH is attained around 153 HRB (2D and 3D plots) at a TRS of 1500 rpm and an AL of 5 kN.

Figure 11 represents the interaction effect of AL along with WS at constant TRS of 1500 rpm. The optimum value of the optimum WNH of 152 HRB (2D and 3D plots) is obtained at a WS of 37.5 mm/min and an AL of 5 kN.

Figure 12 presents the hardness survey analysis for Optimum Conditions at TRS of 1451.67 rpm, WS of 42.22 mm/min, and AL of 5.29 kN). It shows that the lowest hardness is recorded at the HAZ region of retreating side. Retreating side (RS) records appreciably lower hardness values compared to advancing side (AS). The joint records the highest hardness value of 154 HRB in the weld nugget region.

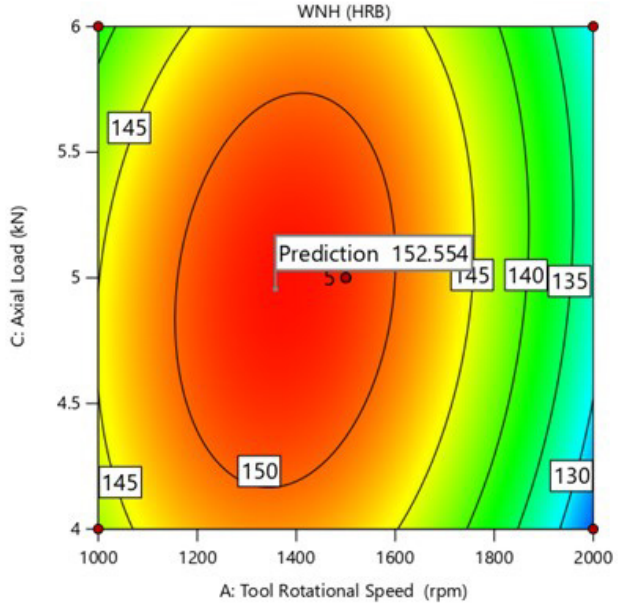

(a) 2D Contour plot

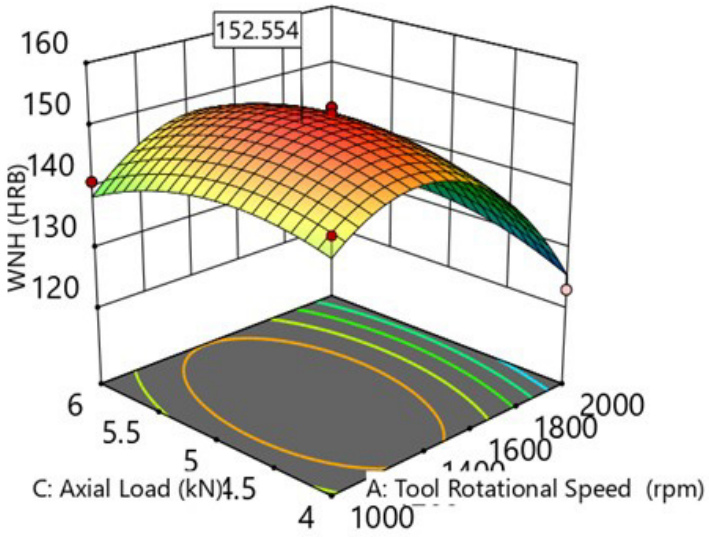

(b) 3D Contour plot

Figure 10. Contour plots (influence of TRS and AL on WNH.

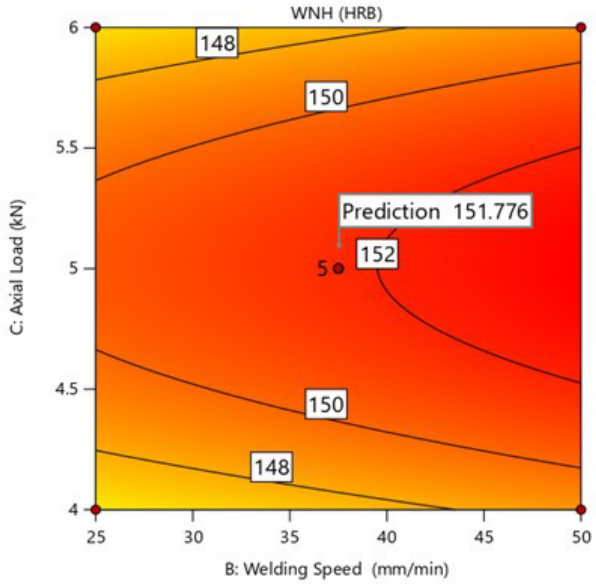

(a) 2D Contour plot

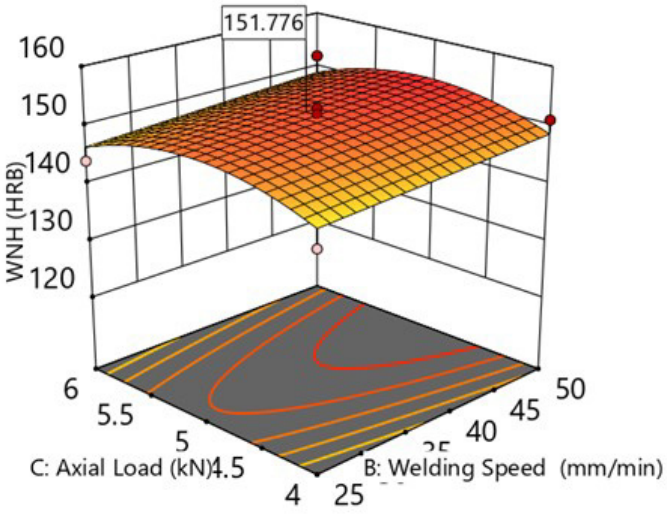

(b) 3D Contour plot

Figure 11. Contour plots (influence of WS and AL on WNH.

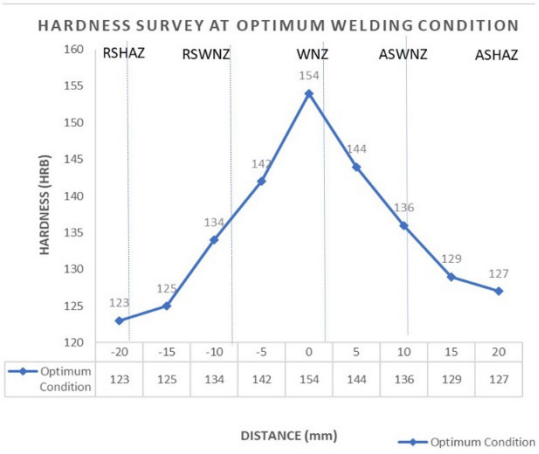

Figure 12. Hardness survey analysis for Optimum Conditions (TRS of 1451.67 rpm, WS of 42.22 mm/min, and AL of 5.29 kN).

4.1.3. Results of optimization

After conducting the optimization study for achieving the desired mechanical property on the welded joint, the following optimum welding conditions are selected by optimization criteria as shown in Table 7. From the results obtained from experiments and optimization, it is very clear that the TRS be around 1500 rpm to attain optimum UTS and WNH and showing that these responses mainly depend on TRS compared to other input parameters. The Optimized FSW process parameters and responses predicted by design expert software is shown in Table 8. Figure 13a-d shows the contour plot and overlay plot, which predict the optimum UTS of 465.6 MPa and WNH of 151.8 HRB obtained at the optimum welding conditions such as TRS of 1451.67 rpm, WS of 42.22 mm/min, and AL of 5.29 kN.

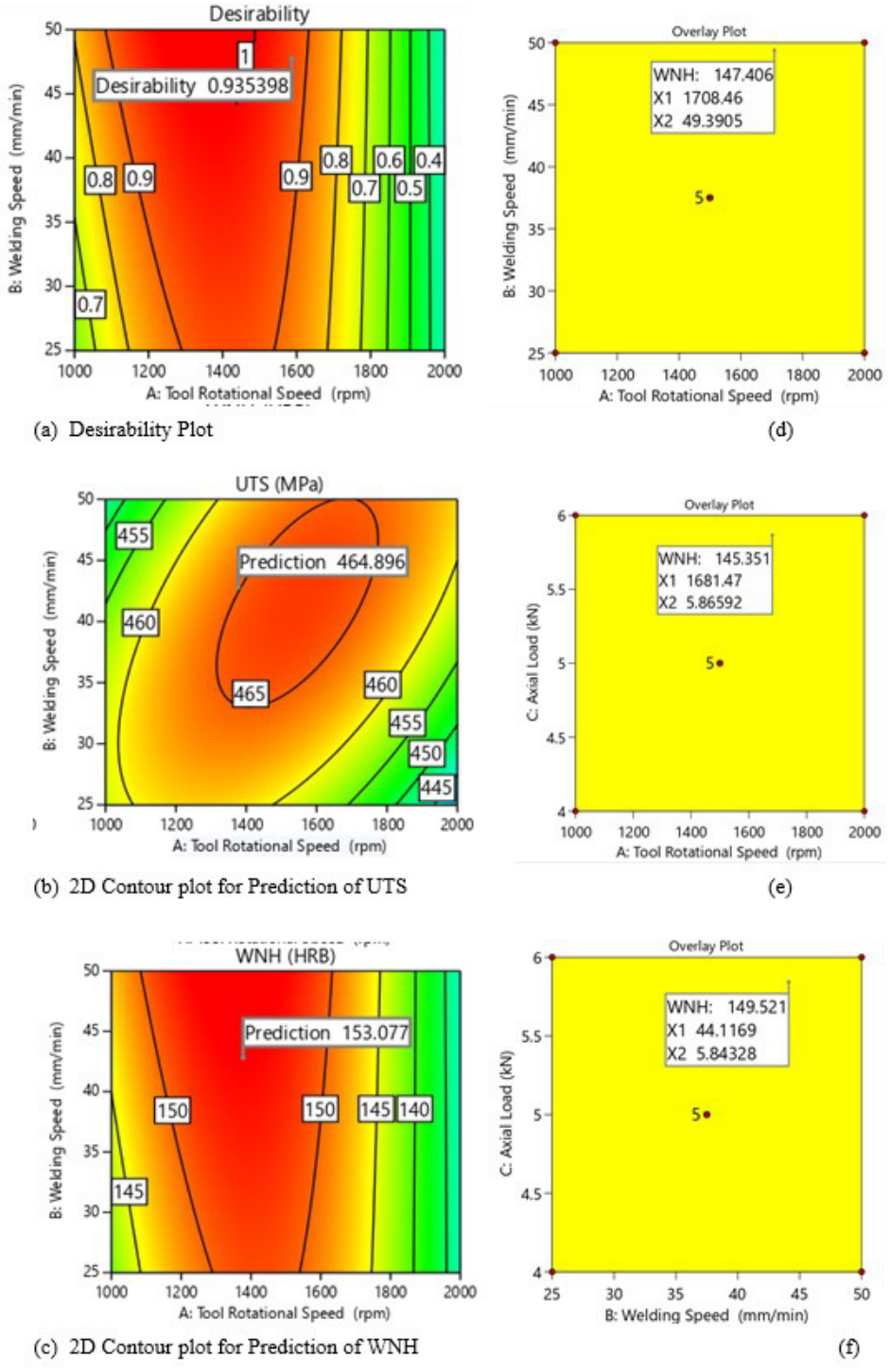

Figure 13. Contour plot (a-c), overlay plot (d-f), and prediction plot for UTS and WNH.

Table 7. Optimization criteria used in this work.

Process Parameters / Responses	Goal	Minimum Limit	Maximum Limit	Importance
Tool Rotational Speed	**is in range**	**1000**	**2000**	**3**
Welding Speed	is in range	25	50	3
Axial Load	is in range	4	6	3
Tensile Strength	maximize	436	468	5
Hardness	maximize	123	153	5

Table 8. Optimized FSW process parameters and responses predicted by design expert software.

Sample	Tool rotational speed (rpm)	Welding Speed (mm/min)	Axial load (kN)	UTS (MPa)	Microhardness HRB
1	1451.67	42.22	5.29	465.6	151.8

4.1.4. Validation for the developed model

The empirical or mathematical model established by the desirability approach is compared with experimental results and the errors are calculated for all seventeen runs (Table 2). The experimental value, predicted value, and error in percentage for UTS and weld nugget hardness is shown in Table 9. The experimental values are calculated by conducting the experiments and the predicted values are determined from the empirical equations developed by the design expert software. For UTS, the error in percentage is in the range from -0.873 to +2.849 and for WNH, the percentage of error is in the range of - 1.13 to + 1.69. Hence the newly developed model confirms that the predicted value of UTS and WNH is almost equal to the experimental values.

Table 9. Experimental and Predicted values for seventeen runs.

Run	UTS (MPa)			WNH (HRB)		
	Experimental Value	Predicted Value	Error in %	Experimental Value	Predicted Value	Error in %
1	466	466.25	0.054	153	154.625	1.06
2	465	467.25	0.484	152	153.25	0.82
3	450	447.75	-0.500	127	128.75	1.38
4	452	455.75	0.830	142	141.75	-0.18
5	436	438.5	0.573	138	139.75	1.27
6	458	454.	-0.873	143	141.5	-1.05
7	443	444.2	0.271	151	151.75	0.50
8	452	453.2	0.265	141	139.4	-1.13
9	454	455.2	0.264	142	144.4	1.69
10	466	467.2	0.258	153	154.75	1.14
11	464	465.2	0.259	144	152.4	5.83
12	466	468.25	0.483	152	154.5	1.64
13	468	468.5	0.107	151	150.25	-0.50
14	456	457.25	0.274	123	122.25	-0.61
15	465	478.25	2.849	150	151.25	0.83
16	454	456.75	0.606	146	147.75	1.20
17	465	467.75	0.591	132	131.75	-0.19

The results of validation experiments are shown in Table 10. For predicted optimal welding condition, this predicted model is also employed for validation. Three confirmation experiments have been performed with a TRS of 1451.67rpm, WS of 42.22 mm/min, and an AL of 5.29 kN. The maximum percentage of error for the prediction of optimum UTS and WNH are + 0.30 and + 0.99 respectively.

Table 10. Validation of test results.

Run	Tool Rotational Speed (rpm)	Welding Speed (mm/min)	Axial Load (kN)	UTS (MPa)		Error in %	Weld Nugget Hardness (HRB)		Error in %
				Actual value	Predicted value		Actual value	Predicted value	
1	1451.67	42.22	5.29	464	465.6	-0.34	154	151.8	-0.33
2	1451.67	42.22	5.29	466	465.6	0.086	153	151.8	0.32
3	1451.67	42.22	5.29	467	465.6	0.30	153	151.8	0.99

4.2. Microstructural characterization

Figure 14a depicts the presence of coarse grains in the base alloy material (AA6092), along with the dendrite structure resulting from the stir casting technique. On the other hand, Figure 14b illustrates the macrostructural analysis of the FS welded joint. The cross-weld microstructure of FS welded AA6092 joints in Figure 14b-d reveals four distinct zones: the weld nugget zone (WNZ), thermo-mechanically affected zone (TMAZ), heat-affected zone (HAZ), and unaffected zone (base material). It also shows the absence of micron-level defects, attributed to adequate heat generation and proper plastic flow of the material. Additionally, the grains observed are noticeably finer in comparison to the grains in the base metal. Notably, the microstructure and grain size differ significantly in the WNZ, TMAZ, and HAZ, which can be attributed to the varying heating and cooling experienced during the FSW process. Specifically, the weld nugget zone exhibits finer grains compared to the TMAZ, HAZ, and unaffected zone. Additionally, the photomicrograph highlights the presence of fine recrystallized structures within the WNZ. An interesting observation is that the coarse grain structure observed in the base material (Figure 14a) transforms into a finer grain structure due to the mechanical stirring action of the FSW tool, as shown in Figure 14d. This change in grain structure is a result of the FSW technique's influence on the microstructure of the welded material.

Figure 15a-d showcases the SEM micrographs of the base material and the FS welded alloy. In Figure 15a, show the grain size in the base material (AA6092). Moving to Figure 15b, a clear depiction of the four different zones (TMAZ, WNZ, HAZ, and unaffected zone) within the FS welded alloy is observed. Figures 15c-d provide compelling evidence that the weld nugget zone exhibits a fine grain structure in comparison to the

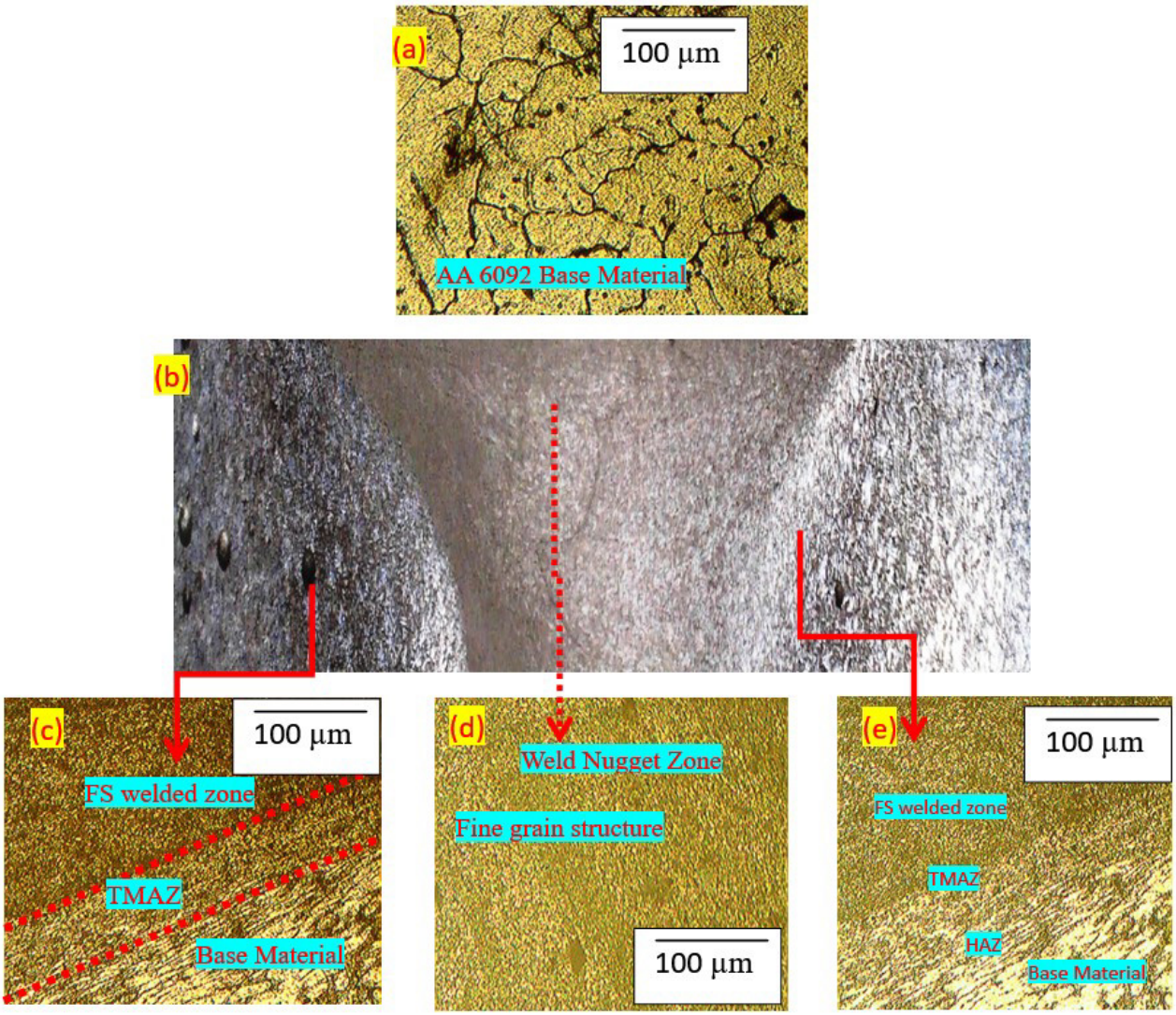

Figure 14. (a) Microstructural analysis of base material, (b) Macrostructural analysis of FS welded alloy and (c-e) Microstructural analysis of FS welded alloy.

TMAZ, HAZ, and unaffected zone. These micrographs highlight the presence of fine grain that obtain due to stirring action of non-consumable rotating tool. This rotating tool create both high plastic deformation and high temperature which cause dynamic recrystallization of grains. This dynamic recrystallization of grains and fine grain structure enhances UTS of the FS welded joints with lower ductility. These grain structures act as barriers to dendritic growth at the grain boundaries. The inhibition of dendritic growth leads to an improvement in the ultimate tensile strength (UTS) and microhardness of base alloy. Additionally, the micrographs illustrate the degree of accumulation of clusters and their growth contributing significantly to the overall strength of alloys.

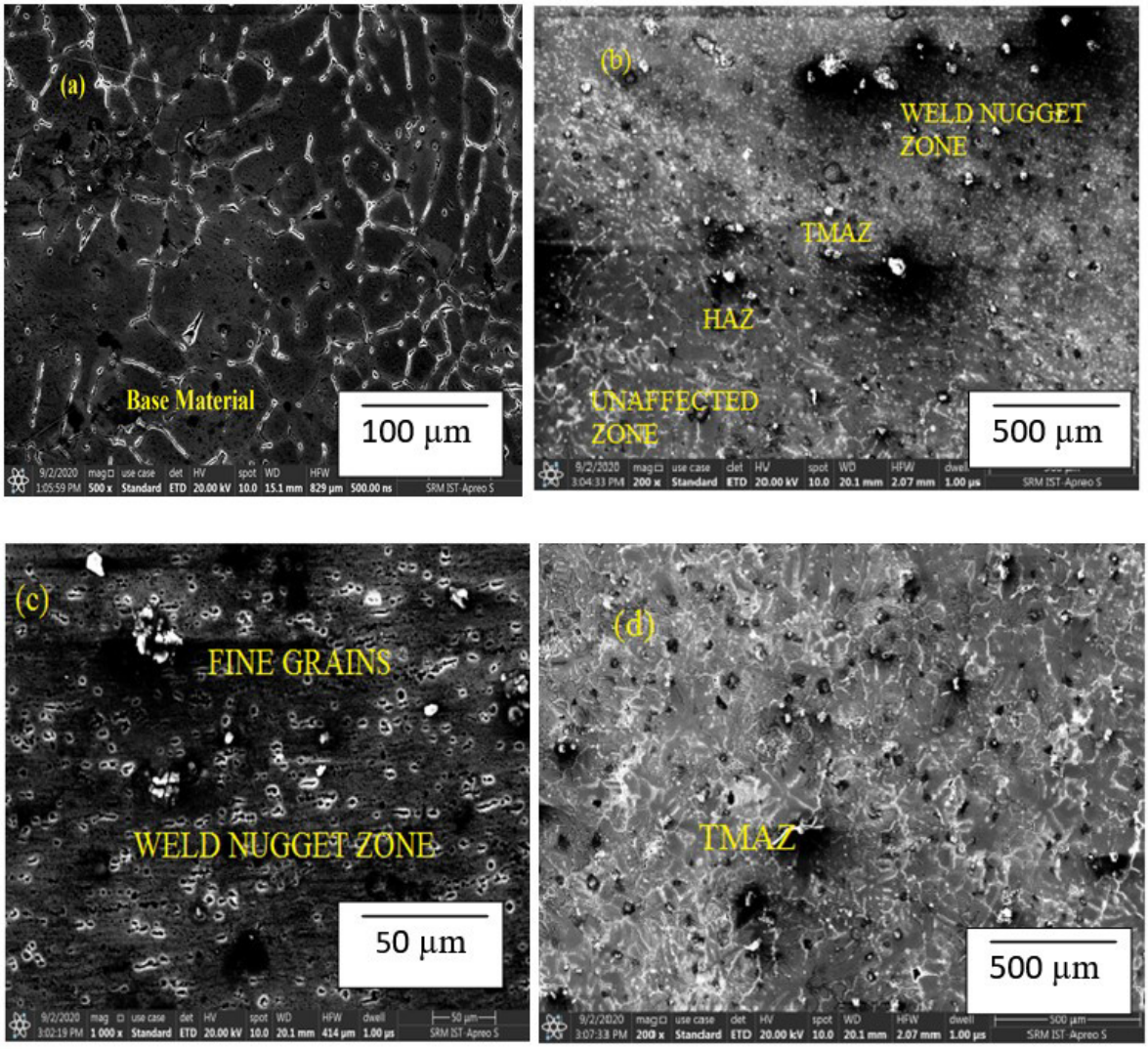

Figure 15. (a-d) SEM analysis of base material and FS welded alloy.

After validating the results, SEM analysis was conducted on the fractured tensile specimen of FS welded AA6092 material with optimized parameters. The analysis reveals that the joint, which is created with FSW parameters set at TRS of 1451.67 rpm, at WS of 42.22 mm/min and at AL of 5.29 kN, exhibits superior strength characteristics in comparison to the other joints. The SEM image provided above corresponds to this specific parameter configuration. The SEM report in Figure 16a-c illustrates the microstructure of the fractured tensile specimen, clearly indicating two distinct regions: the non-fracture surface region and the fracture surface region. The fracture surface exhibits a fibrous appearance or display a matte or silky texture and the centre of the fracture surface shows equiaxed dimples. Figure 16a depicts the fracture surface, which was further magnified to 50 µm and 100 µm, as shown in Figure 16b and Figure 16c, respectively. These magnified images reveal the presence of dimples, which are characteristic of ductile fracture behavior. Notably, the size of these dimples is smaller on the fracture surface of the stir zone when compared to the base alloy. Smaller dimples indicate that there is higher ultimate tensile strength (UTS) and microhardness in stir zone when compared to the base alloy.

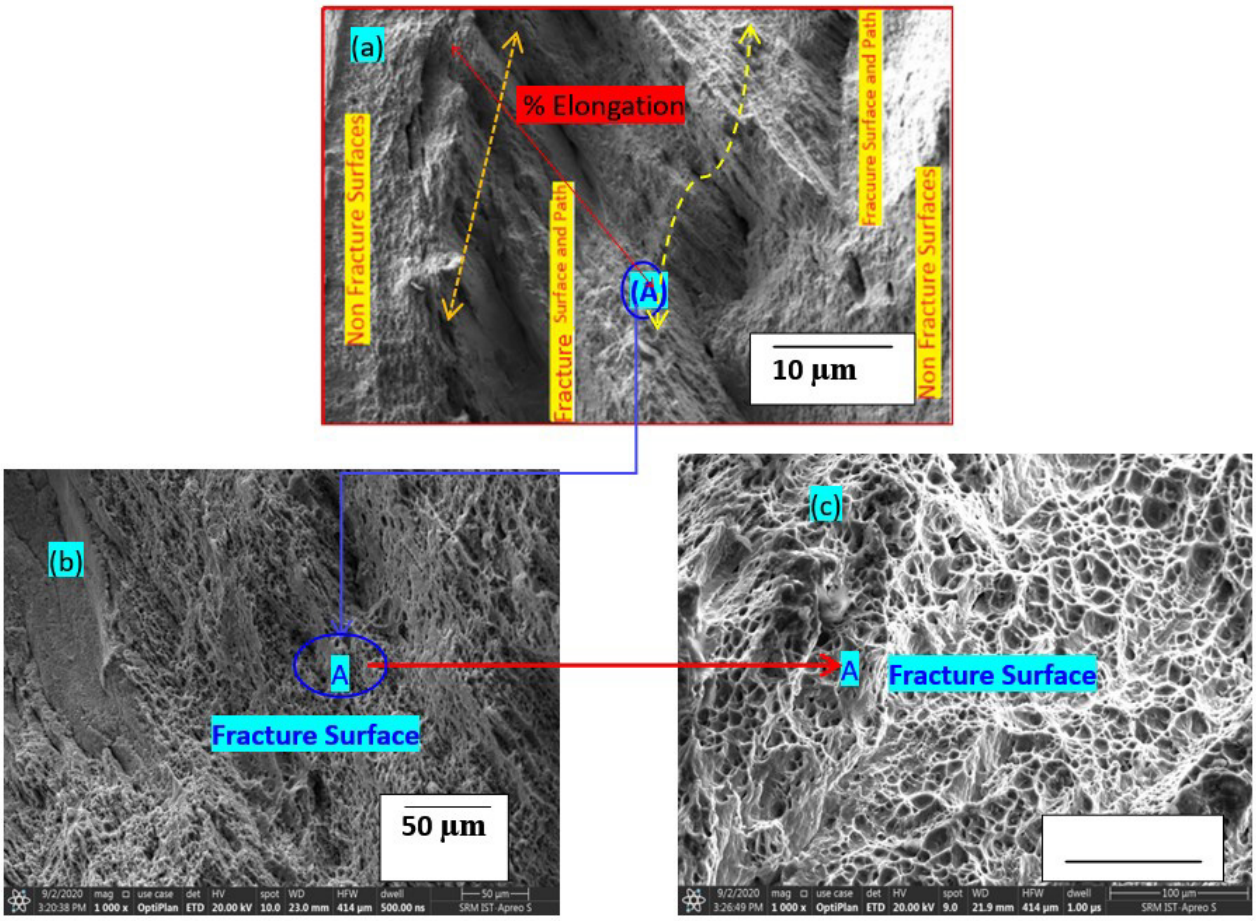

Figure 16. (a-c) SEM Fracto**graphic ana**lysis for the tensile specimen of FSW joint.

5. Conclusions

In this current study, experiments are conducted involving various critical process parameters, namely TRS, WS, and AL, using multiple trials. Additionally, the FSW process parameters are optimized for AA6092 alloy and arrived at the following key findings:

1. The desirability approach is further employed successfully from the result of all seventeen experiments designed by the Box–Behnken method;
2. Box–Behnken's three-factorial experimental design is utilized to establish correlations between the responses, specifically UTS (Ultimate Tensile Strength) and WNH (Weld Nugget Hardness), and the input parameters, which include TRS, WS, and AL. The optimal UTS and WNH values were determined to be 465.6MPa and 151.8 HRB, respectively. These values were achieved under the following welding conditions: TRS of 1451.67 rpm, WS of 42.22 mm/min, and an AL of 5.29 kN;
3. The perturbation plots as well as 2D and 3D contour plots, which were analysed to assess the interaction effects of the welding parameters. This analysis was conducted using Design Expert software;
4. A newly devised model was established and validated, demonstrating a high degree of consistency between the predicted values of UTS and WNH and the corresponding experimental results. The maximum percentage of error observed is merely + 2.849% for UTS and + 1.69% for WNH;
5. The microstructural and SEM analysis of FSW joints provided compelling evidence that the weld nugget zone exhibits a significantly finer grain structure in comparison to the TMAZ, HAZ, unaffected zone, and base alloy. This leads to an improvement in the ultimate tensile strength (UTS) and microhardness of base alloy in the weld nugget zone.

Authors' contributions

UMJ: conceptualization, data curation, formal analysis, investigation, methodology, resources, software, supervision, validation, writing – original draft, writing – review & editing.

References

[1] Guo JF, Chen HC, Sun CN, Bi G, Sun Z, Wei J. Friction stir welding of dissimilar materials between AA6061 and AA7075 Al alloys effects of process parameters. Materials & Design. 2014;56:185-192.

[2] Sreenivas P, Kumar AR, Sreejith PS. Effect of applied axial force on FSW of AA 6082 - T6 aluminium alloys. International Journal of Mechanical Engineering and Technology. 2017;8(1):88-99.

[3] Farzadi A, Bahmani M, Haghshenas DF. Optimization of operational parameters in friction stir welding of AA7075-T6 aluminum alloy using response surface method. Arabian Journal for Science and Engineering. 2017;42):4905-4916. http://dx.doi.org/10.1007/s13369-017-2741-6.

[4] Verma S, Gupta M, Misra JP. Optimization of process parameters in friction stir welding of armor- marine grade aluminium alloy using desirability approach. Materials Research Express. 2018;6(2):026505. http://dx.doi.org/10.1088/2053-1591/aaea01.

[5] Arab M, Zimri M. Optimization of process parameters on friction stir welding of AA6082-T6 butt joints using taguchi method. Mechanics, and Mechanical Engineering. 2018;22(4):1371-1380. https://doi.org/10.2478/mme-2018-0107.

[6] Khaki S, Heidari A, Kolahdooz A. Optimizing friction stir welding process for enhancing strength and hardness using Taguchi multi-objective function method. Int J Advanced Design and Manufacturing Technology. 2019;12(3):25-33.

[7] Mishra RS, Jain S. Friction Stir Welding (FSW) process on aluminum alloy 6082-T6 using Taguchi technique. International Journal of Research in Engineering and Innovation. 2019;3(5):301-305. http://dx.doi.org/10.36037/IJREI.2019.3503.

[8] Sameer MD, Birru AK. Investigations on microstructural evolutions and mechanical properties of dual-phase 600 steel and AA6082-T6 Aluminum Alloy dissimilar joints fabricated by friction stir welding. Transactions of the Indian Institute of Metals. 2019;72:353-367. http://dx.doi.org/10.1007/s12666-018-1487-5.

[9] Khanna N, Bharati M, Sharma P, Badheka VJ. Design-of-experiments application in the friction stir welding of aluminium alloy AA 8011-h14 for structural application. Multidiscipline Modeling in Materials and Structures. 2020;16(3):606-622. http://dx.doi.org/10.1108/MMMS-07-2019-0130.

[10] Maneiah D, Mishra D, Rao KP, Raju KB. Process parameters optimization of friction stir welding for optimum tensile strength in Al 6061-T6 alloy butt welded joints. Materials Today: Proceedings. 2020;27(2):904-908. http://dx.doi.org/10.1016/j.matpr.2020.01.215.

[11] Acharya U, Roy BS, Saha SC. A study of tool wear and its effect on the mechanical properties of friction stir welded AA6092/17.5 SiCp composite material joint. Materials Today: Proceedings. 2018;5(3):20371-20379. http://dx.doi.org/10.1016/j.matpr.2018.06.412.

[12] Acharya U, Roy BS, Saha SC. Effect of tool rotational speed on the particle distribution in friction stir welding of AA6092/17.5 SiCp-T6 composite plates and its consequences on the mechanical property of the joint. Defence Technology. 2020;16(2):381-391. https://doi.org/10.1016/j.dt.2019.08.017.

[13] Umar Mohamed J, Palaniappan PLK, Maran P. Influence of post weld heat treatment on the tensile and microhardness characteristics of friction stir welded joints of AA6082/ZrO_2/B_4C composites. Materials Today: Proceedings. 2022;56:56. http://dx.doi.org/10.1016/j.matpr.2022.02.535.

[14] Pandiyarajan R, Maran P, Murugan N, Marimuthu S, Sornakumar T. Friction stir welding of hybrid AA 6061-ZrO_2-C composites FSW process optimization using desirability approach. Materials Research Express. 2019;6(6):066553. http://dx.doi.org/10.1088/2053-1591/ab084e.

[15] Periyasamy P, Mohan B, Balasubramanian V, Rajakumar S, Venugopal S. Multi-objective optimization of friction stir welding parameters using desirability approach to join Al/SiCp metal matrix composites. Transactions of Nonferrous Metals Society of China. 2013;23(4):942-955. http://dx.doi.org/10.1016/S1003-6326(13)62551-0.

[16] Umar Mohamed J, Palaniappan PLK, Maran P, Pandiyarajan R. Investigation and optimization of friction stir welding process parameters of stir cast AA6082/ ZrO_2 / B_4C composites'. Materials Science Poland. 2020;38(4):715-730.

[17] Umar Mohamed J, Palaniappan PLK, Maran P, Pandiyarajan R. Influences of ZrO_2 and B_4C reinforcement on metallurgical, mechanical, and tribological properties of AA6082 hybrid composite materials. Journal of Ceramic Processing Research. 2021;22(3):306-316. http://dx.doi.org/10.36410/jcpr.2021.22.3.306.

[18] Salih OS, Ou H, Wei X, Sun W. Microstructure and mechanical properties of friction stir welded AA6092/SiC metal matrix composite. Materials Science and Engineering A. 2019;742:78-88. http://dx.doi.org/10.1016/j.msea.2018.10.116.